vortex briefly, and make 25 mL aliquots in 50-mL tubes. Leave at room temperature for a short time and tighten tube caps. Store agarose gels at 4 °C until use.

APS (10%): dissolve 1.7 g APS in 17 mL MilliQ water before use. For the composition of SDS-PAGE buffers refer to our previous report[29]. The light and heavy solutions contain 10% and 15% bis-acrylamide, respectively.

▲ CRITICAL Add 10% APS and TEMED just before pouring the solution into the DALT Gradient Maker; gels will be partially polymerized in the GiantGelCaster within 10 min.

Bind-Silane solution: mix 10 μL Bind-Silane, 200 μL glacial acetic acid, 8 mL ethanol, and 1.8 mL MilliQ water.

Electrode buffer for SDS-PAGE: for six GiantGelRunners (12 gels), dissolve 105 g of Tris-HCl and 510 g of glycine in 30 L MilliQ water, add 350 mL 10% SDS. Make up to 35 L with MilliQ water.

In-gel digestion wash buffer 1: 50% methanol. Mix methanol with an equal volume of MilliQ water.

In-gel digestion wash buffer 2: 50 mM ammonium bicarbonate. Dissolve 395 mg ammonium bicarbonate in 100 mL MilliQ water.

In-gel digestion wash buffer 3: 50 mM ammonium bicarbonate, 50% acetonitrile. Dissolve 395 mg ammonium bicarbonate in 50% acetonitrile.

In-gel digestion dehydration buffer 1: 50% acetonitrile. Mix acetonitrile with an equal volume of MilliQ water.

In-gel digestion dehydration buffer 2: 100% acetonitrile.

Trypsin solution: add 800 μL of 50 mM ammonium bicarbonate (wash buffer 2) in a tube containing 20 μg Sequence Grade Modified trypsin.

1% TFA: mix 1 mL TFA with 99 mL MilliQ water.

Extraction buffer: 45% acetonitrile, 0.1% TFA. Mix 1800 μL 50% acetonitrile (dehydration buffer 1), and 200 μL 1% TFA.

Dissolving buffer: mix 50 μL of 1% TFA and 450 μL of MilliQ water (0.1% TFA). Mix 10 mL of 100% TCA solution and 90 mL MilliQ water (10% TCA). Store at 4 °C until use.

Luria-Bertani (LB) medium (1L): dissolve 10 g bacto-tryptone, 5 g bacto-yeast extract, and 10 g NaCl in 1 L water; adjust pH to 7.0 with 1N NaOH. Autoclave and store at 4 °C.

LB/Ampicilin plate: dissolve 10 g bacto-triptone, 5 g bacto-yeast extract, and 10 g NaCl in 1 L water. After adjusting the pH to 7.0 with 1 N NaOH, add 15 g bacto-agar and autoclave. Add ampicillin solution (final concentration 100 μg/mL) at 50 °C, dispense the medium into sterilized Petri dishes, and store at 4 °C.

IPTS (100 mM, 10 mL): dissolve 0.24 g IPTG in 10 mL distilled water. Filter with a 0.22-μm filter and store at −20 °C.

X-gal (4%, 10 mL): dissolve 0.4 g X-gal in 10 mL N,N-dimethylformamide and store at −20 °C.

LB/ampicillin/IPTG/X-gal plate: apply 20 μL 100 mM IPTG and 20 μL 4% X-gal to LB/ampicillin plate and spread.

PROCEDURE

Cell preparation

● **Timing: days 1–3**

1| Add 100 μL of 1 μg/mL human fibronectin in D-PBS on a 3-μm porous PET membrane surface in a 12-well culture plate for 30 min at room temperature.

2| Remove fibronectin.

3| Seed 1×10^5 MDA-MB-231 cells/well in 700 μL of L-15 complete medium in the upper chamber of the 12-well culture plate with fibronectin-coated porous membranes; the bottom chamber is filled with 700 μL of NIH3T3-conditioned medium. Culture the cells for two days at 37 °C in a 5% CO_2 incubator.

4| Wash the cells on the porous membrane three times gently with D-PBS.

5| Remove D-PBS using a pipette and cotton swab without touching the cells. You can now proceed to cell body ablation with the excimer laser using the following protocol.

Excimer laser etching

6| In a LASIK system, an argon fluoride (ArF) excimer laser (193 nm, 10 Hz) passes through laser pulse-shaper optics (a pattern mask, collimator lenses, and an image rotator) to be tuned in a Gaussian pattern for LASIK surgery as illustrated in Figure 2.

7| Tune the pulse configuration in a flat pattern by aligning the lenses so that two adjacent laser pulses partially overlap. In this setting, the cumulative laser intensity is constant at any point in the irradiation area and the ablation pattern is horizontally flat within a circle 10-mm in diameter (Figure 2).

8| Adjust the laser pulse energy to 10–14 mJ and the pulse number to 12 per scan.

9| Immediately after absorbing D-PBS from the porous membrane, insert with a cotton swab, and place the insert on the irradiation stage of the tuned LASIK system.

10| Focus the irradiation plane on the surface of the cell monolayer.

11| Start laser scanning monitoring with a CCD camera with oblique illumination.

12| Stop the laser when the light scattering due to cell bodies disappears (record the laser scan number.)

13| Fix the irradiated membrane with formalin and stain it with hematoxylin and eosin.

14| Examine the stained membrane for the remaining cell bodies using a light microscope.

15| Find the minimal laser scan number that provides complete removal of cell bodies (18 to 24 scans are required.)

16| Immediately after complete cell body removal, cut out the irradiated membrane area using a hollow leather punch (5 mm in diameter) and quickly freeze it in liquid nitrogen.

A schematic diagram of laser ablation and protein extraction is presented in Figure 2. In addition, a representative image of the excimer laser scanning of the cells cultured on the porous membrane is provided in Supplementary Video 1.

17| Store the cut membrane at −80 °C until use.

▲ CRITICAL The total protein concentration in the final sample is too low to be measured using conventional methods such as the Bradford or Lowry assays. Thus, we routinely extract proteins from 100 sheets punched out of the ablated porous membranes and analyze them in triplicate 2D gels. An average spot intensity of three gels is then calculated and spots are subjected to further analysis. Sitek et al. reported that 1000 cells were sufficient to generate a 2D image using our protocol [24]. Although the extracts from fewer membrane sheets could generate 2D images, the procedural protein loss is enhanced when the initial protein amount is decreased below a certain level. Although 100 sheets per three gels empirically generate a 2D image with an adequate number of protein spots, the amount of extracted protein can vary among cell types, and we recommend using more membranes if the number of protein spots detected on the 2D gel is less than expected.

Protein extraction

● Timing: day 3, 1 h

18| Extract proteins from pseudopodia in the cut porous membrane (option A) and cell bodies (option B).

A. Extraction of pseudopodial proteins:

i. Macerate 100 frozen membranes.

ii. Rotate macerated membranes in lysis buffer at 4 °C for 15 min.

iii. Centrifuge at ≥ 10,000 g at 4 °C for 5 min to remove insoluble material.

iv. Recover the supernatant and use it in protein expression studies.

B. Extraction of cell body proteins:

i. Scrape 2-day MDA-MB-231 cell monolayers from the porous membrane.

ii. Rotate the scraped cells in lysis buffer at 4 °C for 15 min.

iii. Centrifuge at ≥ 10,000 g at 4 °C for 5 min to remove insoluble material.

iv. Recover the supernatant and use it in protein expression studies.

2D-DIGE

● **Timing: days 3–7 (Figure 3)**—Protein separation by 2D-DIGE, handling of the target gel, and in-gel protein digestion are performed as previously described [29], except the following:

Sample preparation for 2D-DIGE: label the proteins extracted from pseudopodia (option A) and cell bodies (internal control sample; option B) as described in REAGENT SETUP. All procedures should be performed in the dark.

Expect the amount of protein extracted from pseudopodia to be rather small.

Functional analysis of candidate proteins

RNA isolation

● **Timing: day 8**

19| Total RNA was extracted from lysing MDA-MB-231 cells directly in a 10-cm culture dish using TRIzol Reagent according to the manufacturer's instructions[30].

▲ CRITICAL Work with TRIzol Reagent in a chemical fume hood using gloves and eye protection (shield, safety goggles). Avoid inhaling and contact with skin and clothing.

▲ CRITICAL Following centrifugation, the mixture separates into a lower red phenol-chloroform phase, an interphase, and a colorless upper aqueous phase. RNA remains exclusively in the aqueous phase. The volume of the aqueous phase is approximately 60% that of TRIZOL Reagent.

▲ CRITICAL Use 0.5 mL of isopropyl alcohol per 1 mL of TRIZOL Reagent used for homogenization.

▲ CRITICAL Do not dry the RNA by centrifugation under vacuum.

Total cDNA synthesis, polymerase chain reaction, TA cloning, and target cDNA and siRNA synthesis

● **Timing: days 8–X**—All the procedures are performed as previously described [20,31].

Transfection

● **Timing: days X–X+2**

20| Adherent cells are transiently transfected using the Lipofectamine LTX and Plus reagents according to the manufacturer's instructions[32].

Immunostaining and confocal microscopy

● **Timing: days X + 2 (Figure 3)**

21| A total of 1×10^4 MDA-MB-231 cells are cultured on fibronectin-coated porous membrane for 2 days after transfection.

22| Cells are washed 3 times with PBS and fixed with 4% paraformaldehyde at room temperature for 10 min.

23| Membranes are washed 3 times with PBS and permeabilized with 0.25% Triton-X in PBS at room temperature for 5 min.

24| After washing 3 times with PBS, the membranes are incubated in blocking buffer containing 2% bovine serum albumin in PBS for 30 min at room temperature.

25| The membranes are treated with antibodies against the target protein in the blocking buffer overnight at 4 °C.

26| After washing with PBS for 5 min 3 times, the membranes are incubated with Alexa Flour 488-conjugated goat anti-candidate molecule antibody (appropriate dilution) in the blocking buffer for 2 h at 4 °C.

27| After washing 3 times with PBS, phalloidin staining is performed for 20 min at room temperature.

28| The stained membranes are washed 3 times with PBS, mounted, and covered with glass coverslips.

29| The stained cells are examined using a FV1000D IX81 confocal scanning system equipped with 488-nm argon and 568-nm helium-neon lasers. X-YZ vertical sections are generated using a 0.5-mm motor step. Each image represents double-averaged (40–50 line scan) images.

Length and density of pseudopodia

● **Timing: days X + 2**

30| Capture multiple X-Y plane images using a 0.15-μm motor step along the Z-axis.

31| Reconstitute Z-plane views of pseudopodia by stacking the X-Y plane images.

32| Measure the Z-axial length of 200 pseudopodia for each cell type.

33| Measure the area inside the peripheral margin of individual cells in the X-Y planes using ImageJ software.

34| Count the number of pseudopodia present in this area.

35| Analyze 30 cells on the membrane and calculate the pseudopodial density as the total number of pseudopodia divided by the total area occupied by the cells (number/μm^2).

36| Perform triplicate measurements per each cell type and calculate the mean density and standard error.

Timetable

Days 1–3: cell culture on fibronectin-coated porous membranes.

Day 3: sample preparation for 2D-DIGE, 3 h; in-gel sample application, 30 min.

Day 4: first-dimension separation, 1 h, followed by 28 h of electrophoresis; SDS-PAGE gel preparation, 1.5 h, followed by overnight polymerization.

Day 5: second-dimension separation, 2.5 h, followed by overnight electrophoresis.

Day 6: image acquisition, 1.5 h; spot picking, 1 h; in-gel digestion, 6 h, followed by overnight treatment.

Day 7: in-gel digestion, 3 h. Day 8–X: identification of the candidate molecules and cloning of the target genes. Day X: transfection with the cDNA of the target gene.

Day X + 2: observation of pseudopodia using confocal microscopy.

? Troubleshooting

The problems encountered during the procedure such as 2D images with unexpectedly small number of protein spots, low separation of protein spots, and distorted images can be attributed to technical issues with the excimer laser etching and 2D-DIGE. In the excimer laser etching, laser scanning counts should be adjusted according to the cell type and density. For the reproducibility of expression profiling, it is also critical to completely remove cell bodies. In 2D-DIGE, troubleshooting for technical problems such as poor quality of the 2D image can be found in the previous reports[33,34]. The first step in troubleshooting is to determine whether it is the excimer laser etching or 2D-DIGE that has caused the problem. For this purpose, we recommend using an adequate control sample for 2D-DIGE. We have described an established method of protein extraction from cultured cells to be used for 2D-DIGE, and this control protein sample will be helpful to identify the cause of the problem.

Anticipated results

The proposed protocol couples proteomic data with tumor cell invasion activity allowing generation of quantitative information on thousands of proteins from any type of adherent tumor cells. Pseudopodial proteins are candidate biomarkers for evaluation of tumor cell

malignancy potential, and their expression patterns are worth investigating for correlation with clinical and pathological data. Thus, the proposed protocol should contribute to further understanding of tumor invasion and may be used for assessment of cancer invasiveness in clinical settings.

Supplementary Material

Refer to Web version on PubMed Central for supplementary material.

Acknowledgments

This work was supported by grants from the Ministry of Education, Culture, Sports, Science and Technology of Japan; the Nakatani Foundation of Electronic Measuring Technology Advancement; the Ministry of Health, Labor and Welfare, and the Program for Promotion of Fundamental Studies in Health Sciences of the Organization for Pharmaceutical Safety and Research of Japan.

References

1. Lauffenburger DA, Horwitz AF. Cell migration: a physically integrated molecular process. Cell. 1996; 84:359–369. [PubMed: 8608589]
2. Parent CA, Devreotes PN. A cell's sense of direction. Science (New York, NY). 1999; 284:765–770.
3. Guirguis R, Margulies I, Taraboletti G, Schiffmann E, Liotta L. Cytokine-induced pseudopodial protrusion is coupled to tumour cell migration. Nature. 1987; 329:261–263.10.1038/329261a0 [PubMed: 2957596]
4. Yamaguchi H, Condeelis J. Regulation of the actin cytoskeleton in cancer cell migration and invasion. Biochimica et biophysica acta. 2007; 1773:642–652.10.1016/j.bbamcr.2006.07.001 [PubMed: 16926057]
5. Jia Z, et al. Tumor cell pseudopodial protrusions. Localized signaling domains coordinating cytoskeleton remodeling, cell adhesion, glycolysis, RNA translocation, and protein translation. The Journal of biological chemistry. 2005; 280:30564–30573.10.1074/jbc.M501754200 [PubMed: 15985431]
6. Wang Y, Klemke RL. Proteomics method for identification of pseudopodium phosphotyrosine proteins. Methods Mol Biol. 2012; 757:349–365.10.1007/978-1-61779-166-6_21 [PubMed: 21909922]
7. Nguyen TN, Wang HJ, Zalzal S, Nanci A, Nabi IR. Purification and characterization of beta-actin-rich tumor cell pseudopodia: role of glycolysis. Experimental cell research. 2000; 258:171–183.10.1006/excr.2000.4929 [PubMed: 10912799]
8. Mouneimne G, et al. Spatial and temporal control of cofilin activity is required for directional sensing during chemotaxis. Current biology : CB. 2006; 16:2193–2205.10.1016/j.cub.2006.09.016 [PubMed: 17113383]
9. Vadnais J, et al. Autocrine activation of the hepatocyte growth factor receptor/met tyrosine kinase induces tumor cell motility by regulating pseudopodial protrusion. The Journal of biological chemistry. 2002; 277:48342–48350.10.1074/jbc.M209481200 [PubMed: 12372820]
10. Shankar J, et al. Pseudopodial actin dynamics control epithelial-mesenchymal transition in metastatic cancer cells. Cancer research. 2010; 70:3780–3790.10.1158/0008-5472.can-09-4439 [PubMed: 20388789]
11. Wang Y, et al. Profiling signaling polarity in chemotactic cells. Proceedings of the National Academy of Sciences of the United States of America. 2007; 104:8328–8333.10.1073/pnas.0701103104 [PubMed: 17494752]
12. Wang Y, et al. Methods for pseudopodia purification and proteomic analysis. Science's STKE : signal transduction knowledge environment. 2007; 2007:pl4.10.1126/stke.4002007pl4

13. Bantscheff M, Lemeer S, Savitski MM, Kuster B. Quantitative mass spectrometry in proteomics: critical review update from 2007 to the present. Anal Bioanal Chem. 2012; 404:939–965.10.1007/s00216-012-6203-4 [PubMed: 22772140]
14. Beckner ME, Chen X, An J, Day BW, Pollack IF. Proteomic characterization of harvested pseudopodia with differential gel electrophoresis and specific antibodies. Lab Invest. 2005; 85:316–327. 3700239 [pii]. 10.1038/labinvest.3700239 [PubMed: 15654357]
15. Attanasio F, et al. Novel invadopodia components revealed by differential proteomic analysis. Eur J Cell Biol. 2011; 90:115–127. S0171-9335(10)00105-6 [pii]. 10.1016/j.ejcb.2010.05.004 [PubMed: 20609496]
16. Buccione R, Orth JD, McNiven MA. Foot and mouth: podosomes, invadopodia and circular dorsal ruffles. Nature reviews. Molecular cell biology. 2004; 5:647–657.10.1038/nrm1436
17. Reynolds A, Moore JE, Naroo SA, Moore CB, Shah S. Excimer laser surface ablation - a review. Clinical & experimental ophthalmology. 2010; 38:168–182.10.1111/j.1442-9071.2010.02230.x [PubMed: 20398106]
18. Solomon KD, et al. LASIK world literature review: quality of life and patient satisfaction. Ophthalmology. 2009; 116:691–701.10.1016/j.ophtha.2008.12.037 [PubMed: 19344821]
19. Vogel A, Venugopalan V. Mechanisms of pulsed laser ablation of biological tissues. Chemical reviews. 2003; 103:577–644.10.1021/cr010379n [PubMed: 12580643]
20. Ito A, et al. Novel application for pseudopodia proteomics using excimer laser ablation and two-dimensional difference gel electrophoresis. Laboratory investigation; a journal of technical methods and pathology. 2012; 92:1374–1385.10.1038/labinvest.2012.98
21. Unlu M, Morgan ME, Minden JS. Difference gel electrophoresis: a single gel method for detecting changes in protein extracts. Electrophoresis. 1997; 18:2071–2077.10.1002/elps.1150181133 [PubMed: 9420172]
22. Shaw J, et al. Evaluation of saturation labelling two-dimensional difference gel electrophoresis fluorescent dyes. Proteomics. 2003; 3:1181–1195.10.1002/pmic.200300439 [PubMed: 12872219]
23. Berggren K, et al. Background-free, high sensitivity staining of proteins in one- and two-dimensional sodium dodecyl sulfate-polyacrylamide gels using a luminescent ruthenium complex. Electrophoresis. 2000; 21:2509–2521. [pii]. 10.1002/1522-2683(20000701)21:12<2509::AID-ELPS2509>3.0.CO;2-9 [PubMed: 10939466]
24. Kondo T, et al. Application of sensitive fluorescent dyes in linkage of laser microdissection and two-dimensional gel electrophoresis as a cancer proteomic study tool. Proteomics. 2003; 3:1758–1766.10.1002/pmic.200300531 [PubMed: 12973736]
25. Kondo T, Hirohashi S. Application of highly sensitive fluorescent dyes (CyDye DIGE Fluor saturation dyes) to laser microdissection and two-dimensional difference gel electrophoresis (2D-DIGE) for cancer proteomics. Nature Protocols. 2007; 1:2940–2956.10.1038/nprot.2006.421
26. Ito M, et al. alpha-Parvin, a pseudopodial constituent, promotes cell motility and is associated with lymph node metastasis of lobular breast carcinoma. Breast Cancer Res Treat. 201410.1007/s10549-014-2859-0
27. Spence HJ, et al. Krp1, a novel kelch related protein that is involved in pseudopod elongation in transformed cells. Oncogene. 2000; 19:1266–1276.10.1038/sj.onc.1203433 [PubMed: 10713668]
28. Gorg A, Boguth G, Obermaier C, Posch A, Weiss W. Two-dimensional polyacrylamide gel electrophoresis with immobilized pH gradients in the first dimension (IPG-Dalt): the state of the art and the controversy of vertical versus horizontal systems. Electrophoresis. 1995; 16:1079–1086. [PubMed: 7498150]
29. Kondo T, Hirohashi S. Application of highly sensitive fluorescent dyes (CyDye DIGE Fluor saturation dyes) to laser microdissection and two-dimensional difference gel electrophoresis (2D-DIGE) for cancer proteomics. Nature protocols. 2007; 1:2940–2956.10.1038/nprot.2006.421
30. Hagiyama M, Ichiyanagi N, Kimura KB, Murakami Y, Ito A. Expression of a soluble isoform of cell adhesion molecule 1 in the brain and its involvement in directional neurite outgrowth. The American journal of pathology. 2009; 174:2278–2289.10.2353/ajpath.2009.080743 [PubMed: 19435791]
31. Mimae T, et al. Upregulation of notch2 and six1 is associated with progression of early-stage lung adenocarcinoma and a more aggressive phenotype at advanced stages. Clinical cancer research : an

official journal of the American Association for Cancer Research. 2012; 18:945–955.10.1158/1078-0432.ccr-11-1946 [PubMed: 22190591]

32. Mimae T, et al. Increased ectodomain shedding of lung epithelial cell adhesion molecule 1 as a cause of increased alveolar cell apoptosis in emphysema. Thorax. 201310.1136/thoraxjnl-2013-203867
33. Carrette O, Burkhard PR, Sanchez JC, Hochstrasser DF. State-of-the-art two-dimensional gel electrophoresis: a key tool of proteomics research. Nature protocols. 2006; 1:812–823.10.1038/nprot.2006.104
34. Espina V, et al. Laser-capture microdissection. Nature protocols. 2006; 1:586–603.10.1038/nprot.2006.85

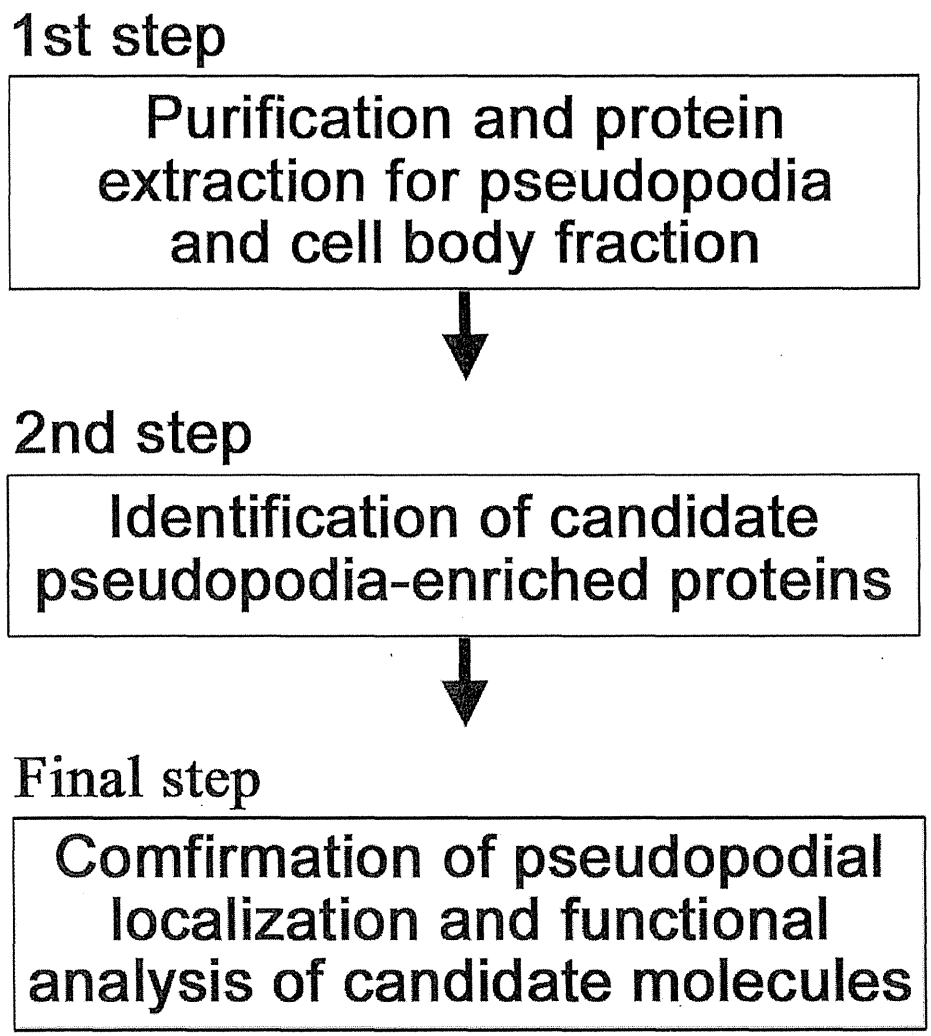

Figure 1.

Flowchart of the experimental steps. The first step is the isolation of pseudopodia and extraction of pseudopodia and cell body proteins. The second step is the identification of pseudopodia-enriched proteins using two-dimensional difference gel electrophoresis (2D-DIGE) and liquid chromatography-mass spectrometry/mass spectrometry (LC-MS/MS). The final step is confirmation of pseudopodia-specific localization and functional evaluation of candidate proteins by confocal imaging.

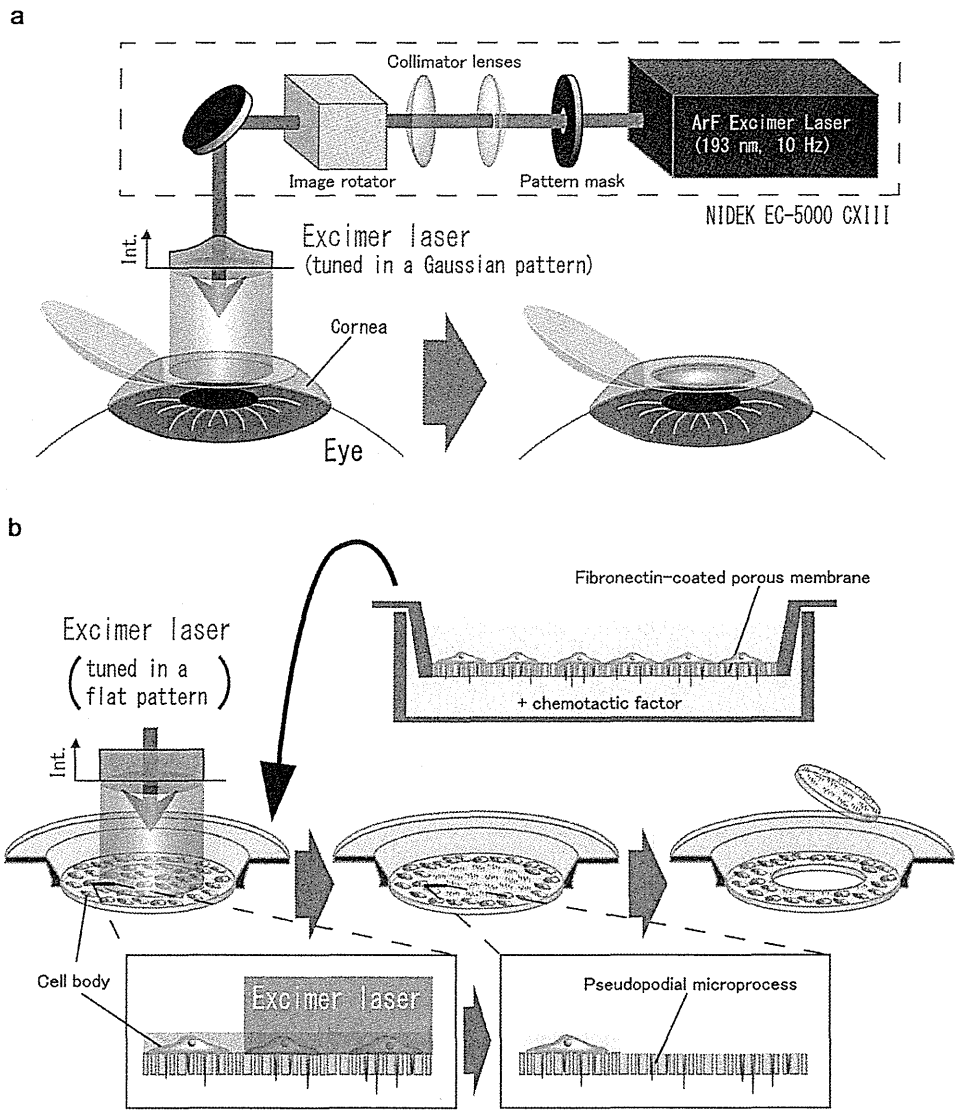

Figure 2. Excimer laser ablation and protein extraction

a. Laser-assisted *in situ* keratomileusis (LASIK). To improve myopia, hypermetropia, and astigmatism, the superficial anterior corneal tissue is reshaped by a topographically assisted excimer laser after the epithelium is flapped from the Bowman's layer. In LASIK, an argon fluoride excimer laser reshapes the superficial anterior corneal tissue in Gaussian fitting without damaging the underlying tissues. b. Pseudopodia isolation and protein extraction. Protein extraction from the membranes containing pseudopodial microprocesses. Cell culture on fibronectin-coated porous membrane positioned over the chemotactic factor-containing medium is shown. The excimer laser ablates the cells on the porous membrane; the laser scanning plane is adjusted to the surface of the porous membrane. The pulse energy and scanning cycles are optimized to completely remove cell bodies and leave pseudopodia intact in the membrane pores. Membranes are punched out after ablation and frozen in liquid

nitrogen. The porous membrane before (left) and after (right) excimer laser ablation is shown.

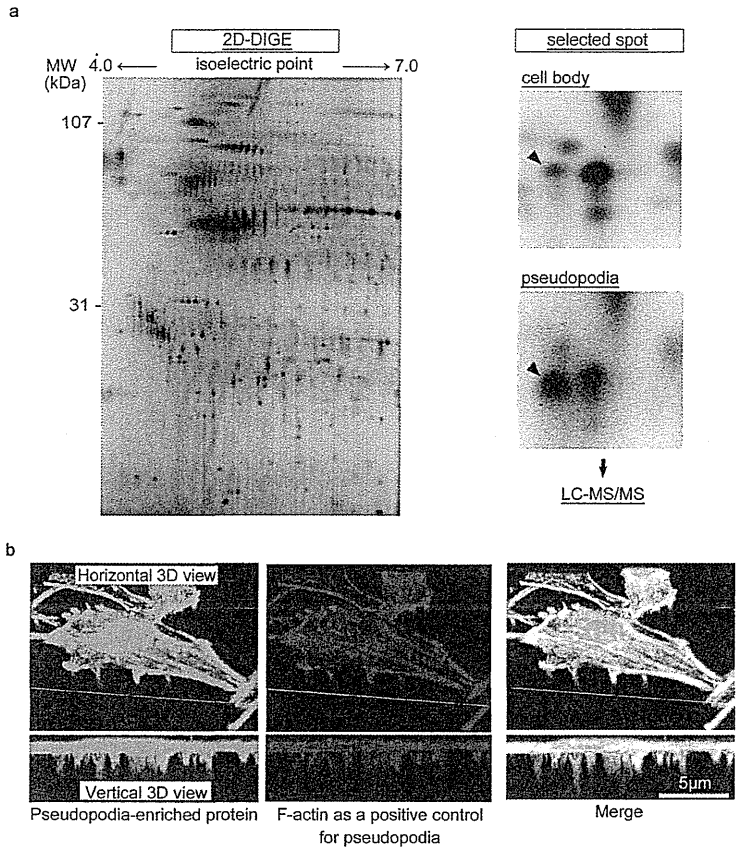

Figure 3. Identification and confirmation about localization of pseudopodia-enriched proteins

a. Identification of pseudopodia-enriched proteins. The proteins purified from pseudopodia and cell bodies are separated by 2D-DIGE, and protein spots are compared based on the relative intensity of fluorescence signals. Proteins spots with signals stronger in the pseudopodial than in the whole cell body fraction are analyzed by LC-MS/MS to identify the candidate pseudopodia-enriched molecules. b. Confirmation of pseudopodia-specific localization and functional analysis of pseudopodia-enriched proteins using immunocytochemical staining. The representative immunocytochemical staining of F-actin with phalloidin to identify pseudopodia and the target candidate protein are shown. In the functional analysis, the length of pseudopodial microprocesses is measured to evaluate the invasiveness/motility of cancer cells with different levels of target protein expression.

EuPA OPEN PROTEOMICS 3 (2014) 183–194

Available online at www.sciencedirect.com

ScienceDirect

journal homepage: http://www.elsevier.com/locate/euprot

Proteomic and meta-transcriptomic study on lymph node metastasis in gastric cancer

Hiroshi Ichikawa[a,b], *Tatsuo Kanda*[c], *Shin-ichi Kosugi*[b], *Yasuyuki Kawachi*[d], *Toshifumi Wakai*[b], *Tadashi Kondo*[a,*]

[a] *Division of Pharmacoproteomics, National Cancer Center Research Institute, 5-1-1 Tsukiji, Chuo-ku, Tokyo 104-0045, Japan*

[b] *Division of Digestive and General Surgery, Niigata University Graduate School of Medical and Dental Sciences, 1-757, Asahimachidori, Chuo-ku, Niigata-shi, Niigata 951-8510, Japan*

[c] *Tsubame Rosai Hospital, 633, Sado, Tsubame-shi, Niigata 959-1228, Japan*

[d] *Nagaoka Chuo General Hospital, 2041, Kawasakimachi, Nagaoka-shi, Niigata 940-8653, Japan*

ARTICLE INFO

Article history:
Received 28 November 2013
Received in revised form
21 February 2014
Accepted 10 March 2014
Available online 15 March 2014

Keywords:
Gastric cancer
Lymph node metastasis
Label-free proteomics
Beta-3 integrin
Transcriptome

ABSTRACT

To examine the proteomic background of lymph node metastasis (LNM) in gastric cancer, we performed protein expression profiling of paired non-tumor, primary tumor, and LNM tissues. Using a label-free proteomic approach, we generated protein expression profiles of 3894 unique proteins and identified 109 differentially expressed proteins. Functional pathway analysis of the differentially expressed proteins showed that members of the beta-3 integrin (ITGB3) pathway were significantly enriched. Aberrations of ITGB3 were reported in various malignancies; however, ITGB3 in LNM tissues has not been examined to date. Different level of ITGB3 expression was confirmed in 20 gastric cancer cases by Western blotting. We analyzed the mRNA levels of the differentially expressed proteins by using a public mRNA expression database; 38.8% of the proteins examined, including those involved in oxidation and reduction, showed correlation between protein and mRNA levels. Proteins without such correlation included factors related to cell adhesion. Our study suggests a novel role for the integrin pathway in the development of LNM in gastric cancer and indicated possible benefits of observational transcriptomic analysis for proteomic studies.

1. Introduction

Gastric cancer is the fourth most common cancer and the second leading cause of cancer-related deaths worldwide [1]. Lymph node metastasis (LNM) is an early event of the metastatic process and is most commonly observed in metastatic gastric cancer [2,3]. The LNM status is one of the most important prognostic factors for gastric cancer, and the 5-year survival rate for LNM-positive gastric cancer is 33.2% [4,5]. These observations suggest that the understanding of the molecular mechanisms of LNM can lead to a novel

* *Corresponding author at*: Division of Pharmacoproteomics, National Cancer Center Research Institute, 5-1-1 Tsukiji, Chuo-ku, Tokyo 104-0045, Japan. Tel.: +81 3 3542 2511x3004; fax: +81 3547 5298.
E-mail address: takondo@ncc.go.jp (T. Kondo).

http://dx.doi.org/10.1016/j.euprot.2014.03.001

prognostic indicator or therapeutic approach for the treatment of gastric cancer.

Metastasis of tumor cells consists of multiple selection steps. Subpopulations of cancer cells with high metastatic potential may migrate from the primary site to distant tissues, where cells adaptive to foreign microenvironments clonally proliferate in metastatic sites [6]. To elucidate the molecular mechanisms underlying these multistage events, genome-wide screening has been performed to identify genetic differences between the primary tumors and the LNM tissues in gastric cancer [7,8]. These studies have suggested the existence of complex genetic abnormalities related to gastric cancer metastasis.

The proteome is a functional translation of the genome. The genomic aberrations of cancer cells are transcribed to the transcriptome, translated to the proteome, then determining cancer phenotypes. In this sense, the proteome is a functional translation of the genome, directly regulating tumor behavior. Proteomic studies can generate unique data about the final products of genome information. The proteomic study has been employed to elucidate the mechanisms underlying LNM development in several types of cancers, and various intriguing findings have been reported [9]. Therefore, the investigations by the proteomic approach will be important clues to understand the molecular mechanisms underlying LNM in gastric cancer. These approaches will further the understanding of biological mechanisms in gastric cancer progression and will eventually benefit cancer patients.

In this study, we aimed to elucidate the proteomic background of LNM in gastric cancer. Protein expression profiles consisting of 3894 unique proteins were generated using sodium dodecyl sulfate (SDS)-PAGE-based protein separation followed by LC–MS/MS. Using a label-free quantification method, we identified 109 differentially expressed proteins in the LNM tissues. Functional pathway analysis demonstrated that proteins involved in the beta-3 integrin (ITGB3) pathway were significantly enriched within LNM, and the expression pattern of ITGB3 in gastric cancer progression and metastasis was examined by Western blotting. The application of meta-transcriptomics revealed the possible trends of proteins with concordant and discordant expression between proteins and mRNA.

2. Material and methods

2.1. Clinical samples

This study included 20 patients with gastric cancer. Matched and unmatched pairs of tumors, non-tumor and LNM tissues were used; paired tissues from two cases were used for proteomic studies, and all samples were used for Western blotting. The patients underwent surgery at Niigata University Medical and Dental Hospital and the affiliated institutions in Niigata prefecture (Nagaoka Chuo General Hospital, Nanbugo General Hospital, Nagaoka Red Cross Hospital, Nippon Dental University Medical Hospital, Niigata City General Hospital, Tachikawa General Hospital, Shibata Hospital, Saiseikai Niigata Daini Hospital, Sakamachi Hospital, Kashiwazaki General Hospital and Medical Center). All patients underwent surgical resection in 2010 and had no history of cancer treatments involving systemic therapy. At the time of surgery, tissue fragments were grossly resected from the primary tumors, and the matched non-tumor mucosa tissues located at least 5 cm away from the tumor margins were collected. All the tissues were immediately snap-frozen in liquid nitrogen and stored at −80 °C until use. The LNM tissues were cut into two pieces; one was embedded in OCT compound (Sakura Finetechnical, Tokyo, Japan) for histological identification of tumor metastasis, and another was used for proteomic study and Western blotting. By staining frozen sections with hematoxylin–eosin, we confirmed that the lymph node metastatic tissues had at least 50% tumor cells. The tumors were classified on the basis of the histological stage, according to the International Union against Cancer tumor-node-metastasis (TNM) classification, 7th edition [10]. The clinicopathological data for 20 cases are presented in Table 1. This study was approved by the Ethical Review Board of the Niigata University Faculty of Medicine, the affiliated institutions of Niigata University Medical and Dental Hospital, and National Cancer Center. Informed consent was obtained from all the patients at each institution.

2.2. Protein expression profiling

Frozen samples were crushed to powder in liquid nitrogen with a Multi-beads shocker (Yasui Kikai, Osaka, Japan) and treated with lysis buffer containing 6 M urea, 2 M thiourea, 3% CHAPS, and 1% Triton X-100. After the mixtures were centrifuged at 15,000 rpm for 30 min, the supernatants were recovered and used in subsequent protein expression studies.

Protein expression profiles were generated by the LC–MS/MS method. Sixty micrograms of each protein sample was separated on a ready-made 12.5% SDS-PAGE gel (ATTO, Tokyo, Japan). Each gel lanes were cut into 48 pieces of equal size by GridCutter (Gel Company, San Francisco, CA) and subjected to in-gel tryptic digestion as described previously [11]. Trypsin digests were subjected to liquid chromatography coupled with analysis with a LTQ-Orbitrap XL mass spectrometer (Thermo Fisher Scientific, San Jose, CA). Acquired MS and MS/MS spectra (Thermo raw files) were analyzed with the Progenesis LC-MS software, version 3.4 (Nonlinear, Dynamics, Newcastle, UK). Profile data of MS scans were transformed to peak lists with respective peak m/z values, intensities, abundances (areas under the peaks), and m/z width. MS/MS spectra were treated similarly.

After selecting one sample as the reference, the retention times of all the other samples used in the experiment were aligned by manually creating three to five landmarks, followed by automatic alignment of all retention times to maximal overlay of the 2D feature maps. Features with only two or three charges were included in further analyses. MS/MS spectra were exported from the Progenesis software as Mascot generic files (mgf) and were used for peptide identification by searching the SWISS-PROT database (*Homo sapiens*, 471,472 sequences in the Sprot_57.5.fasta file) by using the Mascot software (version 2.2; Matrix Science, London, UK). The following search parameters were used: tolerance of two missed trypsin cleavages, variable modifications on the methionine residue (oxidation, +16 Da), maximum precursor ion mass tolerance

Table 1 – Clinical and pathological data of the gastric cancer patients who participated in this study.

Case number[a]	Patient age	Patient sex	Histological differentiation	T status[b]	N status[b]	M status[b]	Number of metastatic nodes	Lymphatic invasion	Vascular invasion	TNM stage[b]
1	76	Male	WD	T4	N3	M1	9	Presence	Presence	IV
2	65	Male	MD	T4	N1	M1	2	Presence	Presence	IV
3	81	Male	WD	T1	N0	M0	0	Absence	Absence	I
4	68	Male	WD	T1	N0	M0	0	Absence	Absence	I
5	70	Male	MD	T2	N0	M0	0	Absence	Absence	I
6	63	Male	MD	T2	N0	M0	0	Absence	Absence	I
7	57	Male	WD	T1	N0	M0	0	Absence	Absence	I
8	72	Male	MD	T3	N0	M0	0	Absence	Absence	II
9	63	Male	MD	T3	N0	M0	0	Absence	Absence	II
10	72	Male	MD	T2	N1	M0	1	Presence	Absence	II
11	81	Male	MD	T3	N1	M0	1	Presence	Absence	II
12	76	Male	WD	T3	N1	M0	1	Presence	Presence	II
13	64	Male	MD	T2	N1	M0	1	Presence	Presence	II
14	56	Male	MD	T3	N3	M0	18	Presence	Presence	III
15	77	Male	MD	T3	N3	M0	12	Presence	Presence	III
16	55	Male	MD	T3	N2	M0	3	Absence	Absence	III
17	76	Male	MD	T3	N3	M0	7	Presence	Presence	III
18	75	Male	MD	T3	N2	M0	3	Absence	Presence	III
19	72	Male	MD	T4	N3	M1	11	Presence	Presence	IV
20	70	Male	WD	T4	N3	M1	12	Presence	Presence	IV

WD, well differentiated; MD, moderately differentiated.

[a] The samples in case 1 and 2 were used to create the protein expression profiles, and those in case 1 to20 were used for Western blotting analysis.

[b] T status, N status, M status and TNM stage were determined according to the International Union against Cancer tumor-node-metastasis (TNM) classification of 7th edition.

of ±10 ppm, and fragment ion mass tolerance of ±0.8 Da. Proteins with a Mascot score of 34 or more were considered as positively identified. Peptide search results were re-imported to the Progenesis software.

For protein quantification, only nonconflicting peptides (i.e., peptides occurring in only one protein) were selected. After summing up the abundances of all the peptides allocated to each protein, the results of 48 fractions were combined in a total analysis set. All the experiments were performed in duplicates, and each number represented an average of two replicates. The processed raw data on protein abundances were normalized by fixing the mean intensity of each sample at one and were presented as a scatter plot; the ratios of mean abundances in two cases between tissue types were calculated using the Expressionist analyst software (GeneData, Basel, Switzerland). We defined the different expression as more than 2.0-fold difference of the mean protein abundance between tissue types. Proteins that showed higher expression in tumor than non-tumor tissues, and also higher expression in LNM than in the tumor tissues, or proteins that showed lower expression in tumors than in the non-tumor tissues, and even lower expression in the LNM tissues were selected as candidate proteins associated with LNM.

2.3. *Pathway analysis*

Pathway analysis of differentially expressed proteins was performed using the Cytoscape software [12] with the Reactome functional interaction (FI) plug-in [13]. The Reactome FI dataset unites interactions from Reactome and those derived from the pathway databases, including KEGG, BioCye, Panther, The Cancer Cell Map (http://cancer.cellmap.org/), and NCI-PID, with pair-wise interactions gleaned from physical protein-protein interactions in human and model organisms, gene coexpression data, protein domain–domain interactions, protein interactions generated from text mining, and GO annotations [13]. To investigate the functions of the network created, pathway enrichment analysis was performed using the Reactome FI plug-in. Pathways with a false discovery rate (FDR) < 0.05 were considered to be significantly enriched.

2.4. *Western blotting*

Protein samples were separated by SDS-PAGE and blotted onto a PVDF membrane. Primary antibodies against ITGB3 (1:1000; BD Bioscience, San Jose, CA) and secondary antibodies against mouse IgG (1:2000, GE Healthcare Biosciences, Uppsala, Sweden) were used, and immunocomplexes were detected using an enhanced chemiluminescence system (ECL Prime Western Blotting Detection Reagents; GE Healthcare Biosciences) and LAS-3000 (Fujifilm, Tokyo, Japan). To normalize the amount of protein loaded in each lane, the same membranes were stained with Ponceau S. The intensity of Western Blot signals and the density of the total lanes stained with Ponceau S were measured using ImageQuant software (GE Healthcare Biosciences), and the relative intensity was calculated by dividing the intensity of Western Blot signals by the optical density of the total lanes.

2.5. *Gene expression analysis*

The microarray and clinical and pathological dataset of 89 gastric cancer cases was obtained from the Gene Expression Omnibus (GEO) database (GSE 4007). This dataset consists of a total of 44,500 probes corresponding to about 30,300 unique genes. Gene expression data of 14 cases that included 14 primary tumor tissues, 14 corresponding LNM tissues, and 5 matched non-tumor mucosae, were selected for the analysis. To compare protein and mRNA expression, we selected probes corresponding to the differentially expressed 109 genes identified in proteomic analysis. We could obtain the expression data of 67 genes. We selected a probe with the highest expression value when multiple ones exist for the identical gene. Additional data processing such as normalization was not performed. Gene expression data were imported to the Expressionist analyst software (GeneData, Basel, Switzerland), and mean expression ratios between different tissue types were calculated. We defined the different expression as more than 1.0 fold difference of the mean expression value between the tissue types.

2.6. *Gene ontology enrichment analysis*

Gene ontology (GO) enrichment analysis was performed using DAVID, version 6.7 [14]. Data related to genes with concordant and discordant mRNA and protein expression were separately uploaded to DAVID, and the background was defined as "*Homo sapiens*". Functional annotation charts were created using "GOTERM_BP_FAT" (collection of broadest GO terms curated from GO annotations dataset). Thresholds were changed to a gene count of two and an EASE score of one (modified Fisher exact P-value). The P-value for each GO term reflects enrichment in the frequency of that GO term in the uploaded gene list, relative to all the genes in the background list. The GO terms were filtered to include enrichments with Benjamini–Hochberg corrected P-values less than 0.20.

2.7. *Statistical analysis*

The Kruskal–Wallis test was performed to compare continuous variables in multiple groups by using the SPSS 11.5 statistical package (SPSS, Chicago, IL), and differences with $P < 0.05$ were considered statistically significant.

3. Results

An overview of the experiment workflow is shown in Fig. 1. First, we generated protein expression profiles of paired non-tumor, tumor, and LNM tissues from cases 1 and 2 (Fig. 1, Table 1). Each protein sample was separated by SDS-PAGE, and the gel lanes were cut to obtain 48 pieces. Trypsin digests were extracted from each gel piece, and subjected to LC–MS/MS. We identified and quantified 109,949 unique peptides corresponding to 3894 nonredundant proteins from six samples in technical duplicates by the Progenesis LC-MS software (Supplementary Tables 1 and 2). To monitor the reproducibility of the whole process (SDS-PAGE separation, in-gel tryptic digestions, LC–MS/MS, and protein quantification), we generated a

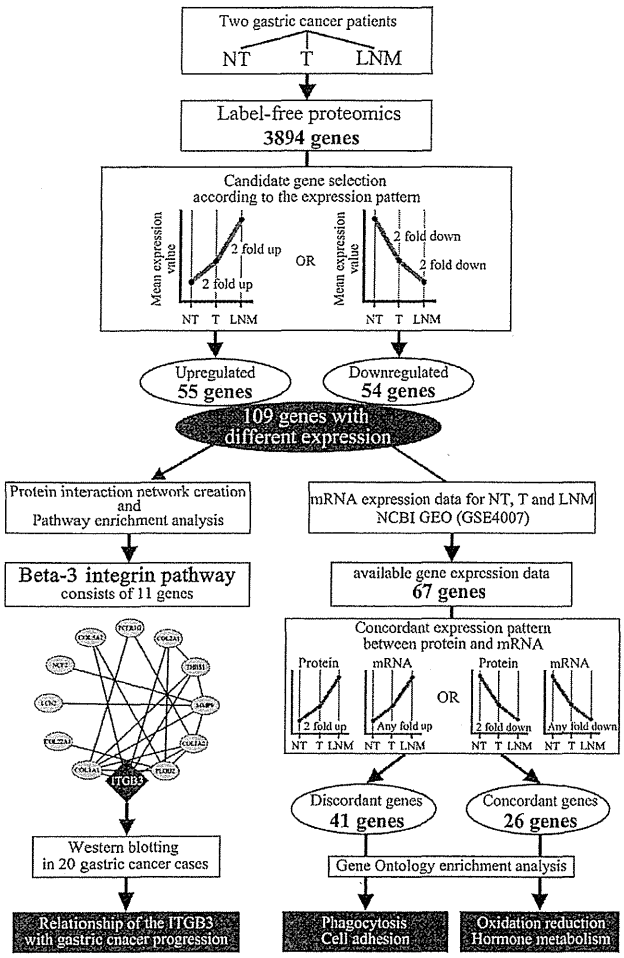

Fig. 1 – Experimental workflow of a label-free proteomics approach with pathway enrichment and mRNA expression meta-analysis. Non-tumor (NT), tumor (T) and lymph node metastasis (LNM) tissues were examined. The label-free quantification method quantified the expression of a total of 3894 proteins; 109 differentially expressed proteins were further analyzed for functional interactions and biological enriched pathways. The beta-3 integrin (ITGB3) pathway was the most enriched pathway in the functional interaction network created. The association between ITGB3 protein expression and gastric cancer progression was confirmed by Western blotting. Among the 109 genes, 67 were grouped according to similarity between the protein and mRNA expression patterns, such as "Concordant genes" or "Discordant genes". Gene ontology analysis showed the enriched functional characteristics in the each gene groups.

scatter plot of technical duplicates from identical samples of the primary tumor tissue from case 2 (Table 1) and calculated the Pearson's correlation coefficient. The scatter plot showed that the normalized abundance of 83.7% and 94.5% of the proteins ranged within 2.0–4.0-fold difference, respectively, and that the correlation coefficient was 0.92 (Supplementary Fig. 1). These results demonstrated high reproducibility of label-free protein expression profiling.

Supplementary Tables 1 and 2 and Fig. 1 can be found, in the online version, at doi:10.1016/j.euprot.2014.03.001.

We compare protein expression profiles between the non-tumor, tumor, and LNM tissues in two cases (Case 1 and 2, Table 1). Among the 3894 proteins, 55 proteins showed significantly (>2-fold ratio of means in two cases) higher expression in tumor than non-tumor tissues and also significantly higher expression in LNM than in the tumor tissues (Fig. 2). In contrast, 54 proteins showed significantly (<2-fold ratio of means in two cases) lower expression in tumors than in the non-tumor tissues, and even significantly lower expression in the LNM tissues (Fig. 3). We selected the 109 differentially expressed proteins as candidate proteins associated with LNM. Details of these proteins are presented in Supplementary Table 3.

Supplementary Table 3 can be found, in the online version, at doi:10.1016/j.euprot.2014.03.001.

We studied the functional interactions of these 109 proteins by using Cytoscape with the Reactome FI plug-in. We found that 11 (10.1%) of the 109 proteins were functionally linked to each other and that the ITGB3 cell surface interactions pathway was the most significantly enriched in the identified network of the 11 proteins (FDR < 1.00E-4, Fig. 4A and Table 2). ITGB3 was identified and examined in our proteomic analysis. ITGB3 protein expression in the LNM tissues was lower than that of the tumor tissues (ratio of means = 3.96), and that of the tumor tissues was higher than that of the non-tumor tissues (ratio of means = 1.76) (Fig. 4B). We validated the relationship between ITGB3 expression and gastric cancer progression in 20 cases by Western blotting. ITGB3 expression was found to significantly increase with cancer stage progression but decrease in LNM tissues (Fig. 4C). These observations confirmed the results of the label-free protein expression profiling.

We analyzed the mRNA levels for the 109 differentially expressed proteins by using a public mRNA expression database. We selected the GSE4007 dataset in the NCBI Gene Expression Omnibus (GEO) because it was the only dataset that included mRNA expression data obtained from paired non-tumor tissues, primary tumor tissues, and LNM tissues, along with sufficient clinical information. From the 109 genes, the mRNA expression data for 67 genes were included in the GSE4007 dataset. Clinical and pathological information and data on mRNA expression have been presented in Supplementary Tables 4 and 5, respectively.

Supplementary Tables 4 and 5 can be found, in the online version, at doi:10.1016/j.euprot.2014.03.001.

To characterize the genes according to the correlation between mRNA and protein expression, we divided the 67 genes into two groups: 26 genes (38.8%) that showed the same protein and mRNA expression patterns were grouped into "Concordant genes" (Table 3), whereas 41 genes that showed different patterns were grouped into "Discordant genes". We analyzed the enriched GO terms in each group by using DAVID, version 6.7. GO terms related to oxidation, reduction, or hormone metabolism were enriched in the group of "Concordant genes", while those involved in phagocytosis or cell adhesion

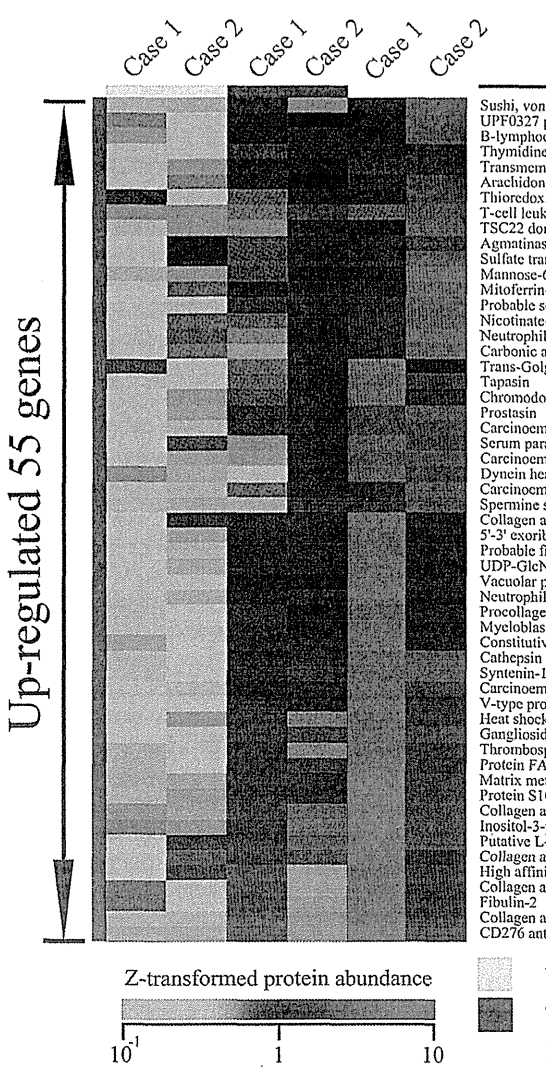

Gene description	Ratio of means (T/NT)	Ratio of means (LNM/T)
Sushi, von Willebrand factor type A, EGF and pentraxin domain-containing protein 1	3.61	4.56
UPF0327 protein C1orf151	3.01	2.28
B-lymphocyte antigen CD20	2.96	2.63
Thymidine kinase 2, mitochondrial	13.59	2.19
Transmembrane glycoprotein NMB	6.14	2.67
Arachidonate 5-lipoxygenase-activating protein	5.11	2.41
Thioredoxin domain-containing protein 6	3.15	3.2
T-cell leukemia/lymphoma protein 1A	88.57	3.65
TSC22 domain family protein 2	2.35	2.31
Agmatinase, mitochondrial	2.91	2.51
Sulfate transporter	2.42	2.07
Mannose-6-phosphate receptor-binding protein 1	2.05	4.34
Mitoferrin-1	4.92	3.04
Probable serine carboxypeptidase CPVL	2.66	2.31
Nicotinate-nucleotide pyrophosphorylase [carboxylating]	2.1	3.75
Neutrophil gelatinase-associated lipocalin	2.09	7.42
Carbonic anhydrase 4	3.7	18.06
Trans-Golgi network integral membrane protein 2	2.84	3.73
Tapasin	102.06	726.07
Chromodomain-helicase-DNA-binding protein 4	2.07	2.49
Prostasin	5.15	5.58
Carcinoembryonic antigen-related cell adhesion molecule 8	22.18	11.22
Serum paraoxonase/arylesterase 2	2.17	3.37
Carcinoembryonic antigen-related cell adhesion molecule 1	3.73	8.84
Dynein heavy chain 2, axonemal	2.27	17.81
Carcinoembryonic antigen-related cell adhesion molecule 5	4.57	4.59
Spermine synthase	2.19	2.59
Collagen alpha-1(XXII) chain	3.21	8.25
5'-3' exoribonuclease 2	13.38	2.36
Probable fructose-2,6-bisphosphatase TIGAR	2.98	2.61
UDP-GlcNAc:betaGal beta-1,3-N-acetylglucosaminyltransferase-like protein 1	10.41	5.4
Vacuolar protein sorting-associated protein 28 homolog	2.99	3.06
Neutrophil cytosol factor 2	4.97	6.98
Procollagen-lysine,2-oxoglutarate 5-dioxygenase 2	11.38	2.7
Myeloblastin	4.37	2.37
Constitutive coactivator of PPAR-gamma-like protein 1	5.68	4.07
Cathepsin H	2.78	3.33
Syntenin-1	2.05	2.61
Carcinoembryonic antigen-related cell adhesion molecule 6	5.59	7.2
V-type proton ATPase 16 kDa proteolipid subunit	7.13	3.73
Heat shock 70 kDa protein 1L	3.16	3.47
Ganglioside-induced differentiation-associated protein 1	3.99	3.09
Thrombospondin-1	2.17	2.79
Protein FAM103A1	2.09	2.79
Matrix metalloproteinase-9	3.46	2.63
Protein S100-A12	2.23	2.12
Collagen alpha-2(V) chain	3.03	2.18
Inositol-3-phosphate synthase 1	4.27	8.3
Putative L-aspartate dehydrogenase	2.76	2.82
Collagen alpha-1(II) chain	3.77	4.16
High affinity immunoglobulin epsilon receptor subunit gamma	2.23	2.08
Collagen alpha-2(I) chain	2.46	2.86
Fibulin-2	2.12	2.48
Collagen alpha-1(I) chain	3.59	2.92
CD276 antigen	2.01	2.25

Fig. 2 – Fifty-five significantly upregulated proteins identified by a label-free quantification method. The protein abundance in each case was z-transformed across all six samples and has been presented in a heatmap format. Tissue types are marked as non-tumor (NT), tumor (T), and lymph node metastasis (LNM). Case numbers correspond to those in Table 1 and Fig. 4. Refer to Supplementary Table 3 for the gene description and values of the ratio of means.

were over-represented in the "Discordant genes" group (Fig. 5 and Supplementary Table 6).

Supplementary Table 6 can be found, in the online version, at doi:10.1016/j.euprot.2014.03.001.

4. Discussion

LNM is one of the most important prognostic factors in gastric cancer, and investigation of the molecular background of LNM formation may lead to novel therapeutic modalities [4]. Metastasis has been assumed to occur through clonal genomic and epigenetic evolution [5]. Molecular mechanisms related to tumor metastasis are upregulated in metastatic tumor cells compared to primary tumors, and exploring differences in the molecular background of primary tumors and LNM tissues may be the most direct and credible way to elucidate the molecular mechanisms underlying the metastasis process.

We employed SDS-PAGE-based size fractionation before mass spectrometry analysis. Pre-fractionation of proteins by SDS-PAGE has significant advantages over other separation techniques in that it detects a greater number of proteins and is widely used to characterize protein complexes in cancer proteomic studies [15–17]. Gel-based size fractionation for the identification of proteins is superior to separation by liquid chromatography as a pre-fractionation method [18]. Jafari et al. compared gel-based protein-separation techniques, including SDS-PAGE, isoelectric focusing with immobilized pH gradient gel strips (IEF-IPG), and two-dimensional PAGE (2D-PAGE), on the basis of their ability to serve as a

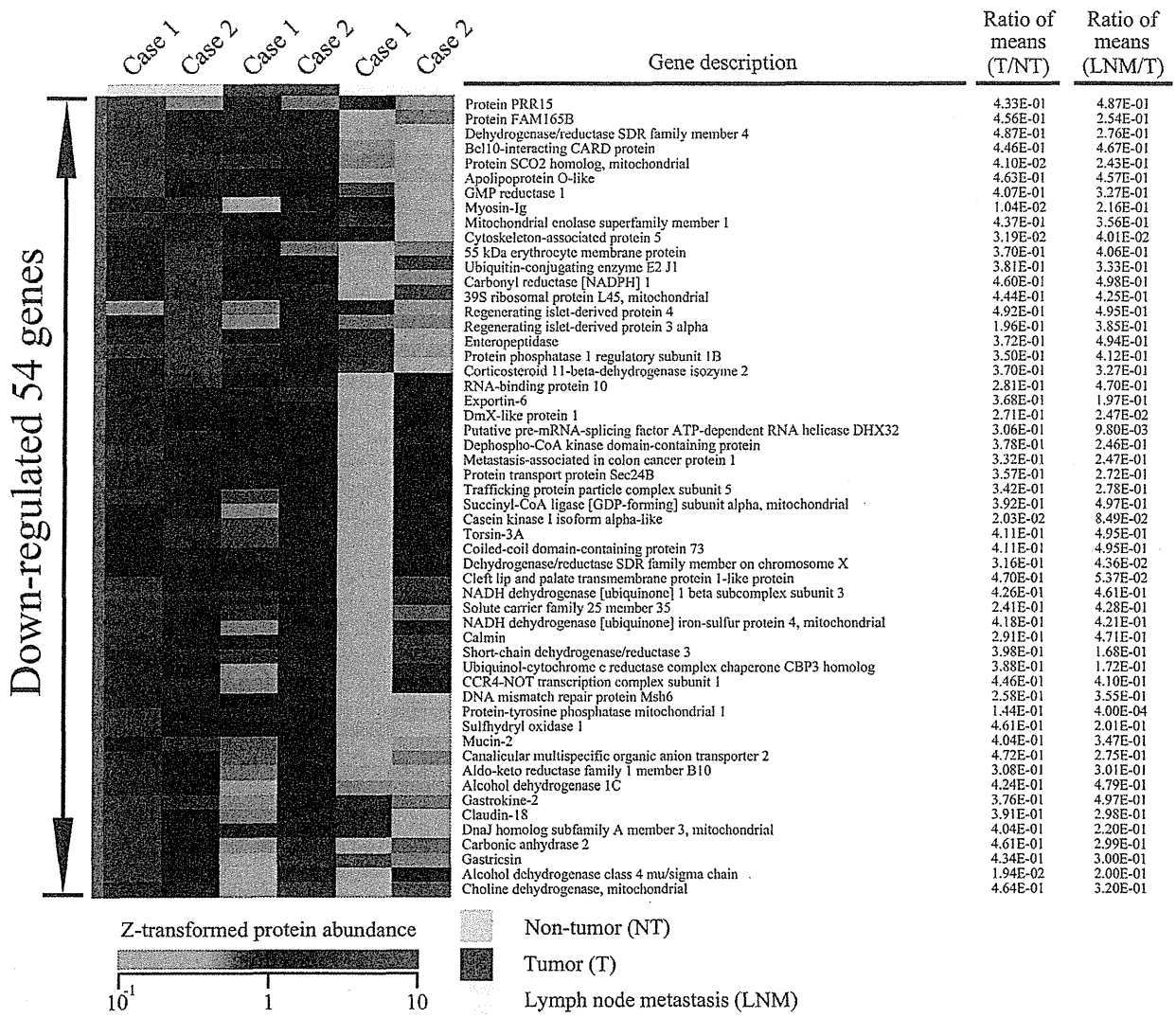

Gene description	Ratio of means (T/NT)	Ratio of means (LNM/T)
Protein PRR15	4.33E-01	4.87E-01
Protein FAM165B	4.56E-01	2.54E-01
Dehydrogenase/reductase SDR family member 4	4.87E-01	2.76E-01
Bcl10-interacting CARD protein	4.46E-01	4.67E-01
Protein SCO2 homolog, mitochondrial	4.10E-02	2.43E-01
Apolipoprotein O-like	4.63E-01	4.57E-01
GMP reductase 1	4.07E-01	3.27E-01
Myosin-Ig	1.04E-02	2.16E-01
Mitochondrial enolase superfamily member 1	4.37E-01	3.56E-01
Cytoskeleton-associated protein 5	3.19E-02	4.01E-02
55 kDa erythrocyte membrane protein	3.70E-01	4.06E-01
Ubiquitin-conjugating enzyme E2 J1	3.81E-01	3.33E-01
Carbonyl reductase [NADPH] 1	4.60E-01	4.98E-01
39S ribosomal protein L45, mitochondrial	4.44E-01	4.25E-01
Regenerating islet-derived protein 4	4.92E-01	4.95E-01
Regenerating islet-derived protein 3 alpha	1.96E-01	3.85E-01
Enteropeptidase	3.72E-01	4.94E-01
Protein phosphatase 1 regulatory subunit 1B	3.50E-01	4.12E-01
Corticosteroid 11-beta-dehydrogenase isozyme 2	3.70E-01	3.27E-01
RNA-binding protein 10	2.81E-01	4.70E-01
Exportin-6	3.68E-01	1.97E-01
DmX-like protein 1	2.71E-01	2.47E-02
Putative pre-mRNA-splicing factor ATP-dependent RNA helicase DHX32	3.06E-01	9.80E-03
Dephospho-CoA kinase domain-containing protein	3.78E-01	2.46E-01
Metastasis-associated in colon cancer protein 1	3.32E-01	2.47E-01
Protein transport protein Sec24B	3.57E-01	2.72E-01
Trafficking protein particle complex subunit 5	3.42E-01	2.78E-01
Succinyl-CoA ligase [GDP-forming] subunit alpha, mitochondrial	3.92E-01	4.97E-01
Casein kinase I isoform alpha-like	2.03E-02	8.49E-02
Torsin-3A	4.11E-01	4.95E-01
Coiled-coil domain-containing protein 73	4.11E-01	4.95E-01
Dehydrogenase/reductase SDR family member on chromosome X	3.16E-01	4.36E-02
Cleft lip and palate transmembrane protein 1-like protein	4.70E-01	5.37E-02
NADH dehydrogenase [ubiquinone] 1 beta subcomplex subunit 3	4.26E-01	4.61E-01
Solute carrier family 25 member 35	2.41E-01	4.28E-01
NADH dehydrogenase [ubiquinone] iron-sulfur protein 4, mitochondrial	4.18E-01	4.21E-01
Calmin	2.91E-01	4.71E-01
Short-chain dehydrogenase/reductase 3	3.98E-01	1.68E-01
Ubiquinol-cytochrome c reductase complex chaperone CBP3 homolog	3.88E-01	1.72E-01
CCR4-NOT transcription complex subunit 1	4.46E-01	4.10E-01
DNA mismatch repair protein Msh6	2.58E-01	3.55E-01
Protein-tyrosine phosphatase mitochondrial 1	1.44E-01	4.00E-04
Sulfhydryl oxidase 1	4.61E-01	2.01E-01
Mucin-2	4.04E-01	3.47E-01
Canalicular multispecific organic anion transporter 2	4.72E-01	2.75E-01
Aldo-keto reductase family 1 member B10	3.08E-01	3.01E-01
Alcohol dehydrogenase 1C	4.24E-01	4.79E-01
Gastrokine-2	3.76E-01	4.97E-01
Claudin-18	3.91E-01	2.98E-01
DnaJ homolog subfamily A member 3, mitochondrial	4.04E-01	2.20E-01
Carbonic anhydrase 2	4.61E-01	2.99E-01
Gastricsin	4.34E-01	3.00E-01
Alcohol dehydrogenase class 4 mu/sigma chain	1.94E-02	2.00E-01
Choline dehydrogenase, mitochondrial	4.64E-01	3.20E-01

Fig. 3 – Fifty-four significantly downregulated proteins identified by a label-free quantification method. The protein abundance of each gene was z-transformed across all 6 samples and has been presented in a heatmap format. The tissue types are marked as shown in Fig. 2. Case numbers correspond to those in Table 1 and Fig. 4. Refer to Supplementary Table 3 for the gene description and values of the ratio of means.

fractionation technique for MS analysis of a complex protein sample [19]. They reported that SDS-PAGE yielded the highest number of identifiable proteins.

In addition, we quantified the identified proteins by a label-free method with the Progenesis LC-MS software. Label-free quantification is widely used because it is a simple technique that allows simultaneous identification and quantification of proteins. Alternatively, isotopic labeling methods such as ICAT [20], iTRAQ [21], and SILAC [22] are also used for MS-based protein quantification; these isotopic labeling methods allow for the comparison of multiple samples in a single LC–MS/MS run, thereby providing increased accuracy, precision, and reproducibility [23]. However, such experiments are complicated because of the additional labeling reactions, and SILAC is available only in tissue culture systems. A label-free method based on Progenesis LC-MS can quantify and identify thousands of proteins from complex samples with a simple technique and high reproducibility. Progenesis LC-MS aligns the ion chromatograms to compensate for variations in retention times among multiple samples before quantification based on ion intensities. It has been reported that analysis of retention time alignment shows similar quantification precision and reproducibility but higher identification capacity than isotope labeling methods such as SILAC [24]. In this study, we identified and quantified 3894 non-redundant proteins from complex clinical samples with high reproducibility (Supplementary Fig. 1) and then employed a label-free quantification method for the proteomic studies.

The development of tumor invasion and metastasis is a very complicated and continuous process with multi steps.